catalysts

MDPI

Article

Reducible Inverse CeO_x-Based Catalyst as a Potential Candidate for Electroreduction

Yongli Shen and Zihui Xiao *

Tianjin Key Laboratory of Advanced Functional Porous Materials, Institute for New Energy Materials & Low-Carbon Technologies, School of Materials Science and Engineering, Tianjin University of Technology, Tianjin 300384, China; ylshen@tjut.edu.cn

* Correspondence: zhxiao@email.tjut.edu.cn

Received: 8 December 2018; Accepted: 23 December 2018; Published: 29 December 2018

Abstract: The inverse metal oxide/metal catalyst is very suitable for electrochemical reaction due to unique catalytic properties of metal oxide with small size and good conductivity of metal. To clarify the potential applications of inverse catalyst in electrochemistry, especially for reducible oxides, an inverse CeO_x/Ag(111) model electrocatalyst was constructed and investigated by Density Functional Theory (DFT) for CO_2 electrochemical reduction. It is found that Ag atoms acting as an electron donor, can partially reduce Ce^{4+} to Ce^{3+} in the supported CeO_x cluster leading to the formation of interfacial Ce^{3+} active sites, which could promote the adsorption and reduction of CO_2. As expected, all elementary reaction involved in the CO_2 electrochemical reduction are more facile on CeO_x/Ag(111) than pure Ag catalyst. Besides, the generation of CH_3OH and CH_4 is favored on CeO_x/Ag(111), whereas the formation of CO, CH_2O and H_2 is obviously suppressed. More importantly, the weak interaction between H_2O and CeO_x cluster is beneficial for the desorption of OH intermediate, which makes the regeneration of the catalyst become easier and result in a great recyclability. All those results demonstrate that CeO_x/Ag(111) is a potential excellent electrochemical catalyst.

Keywords: inverse catalyst; CO_2 electrochemical reduction; CeO_x cluster; DFT; active sites

1. Introduction

Oxide supported metal nanoparticles catalysts are widely used in heterogeneous catalysis and play an important role in industrial production. In the study of the adsorption of H_2 and CO on the oxides supported noble metal catalysts, the different adsorption capacities of H_2 and CO on pre-reduced catalysts at different temperatures was observed, which was attributed to strong metal-support interactions (SMSI) [1]. Long-term studies have shown that this kind of interaction exists only in reductive metal oxides carrier (CeO_2 [2], FeO_x [3]), which is not only act as supports to prevent the sintering of metal nanoparticles but also have a great influence on the catalytic activity of the catalysts. Recently, it is found that the inverse catalysts also exhibit excellent catalytic performance towards some reactions. In all cases, inverse catalysts exhibit strong interaction between the metal and oxide (SMSI) through sharing part of oxygens [4,5]. Density Functional Theory (DFT) research reveals that all Ce atoms are Ce^{3+} in CeO_x/Metal (Cu and Ag) catalyst due to the covalent bond between CeO_x cluster and metal carrier, leading to the formation of mixed oxides in the interface of the catalyst [6]. Thus, it can be speculated that the unique interface in inverse catalysts will play a significant role in the reaction.

At present, studies have shown that the inverse catalysts can catalyze many important reactions such as dissociation of O_2 [5], water-gas shift reaction [7] and CO_2 reduction to produce methanol [8]. The hydrogenation of CO_2 on CeO_x/Cu catalyst indicate that CO_2 molecule can be activated when

it adsorbed on the interface of the catalyst [8]. This inspires that the Ce-related inverse catalysts may be a potential candidate for electrochemical CO_2 reduction reaction (CO_2RR) to produce useful products such as CH_4, CH_3OH, HCOOH or CH_2O. Recently, the DFT investigation about CO_2RR on $(TiO_2)_3/Ag(110)$ have also been carried out. It is demonstrated that the introduction of metal oxides to a metal electrode provides the interfacial active sites for adsorption and activation of CO_2 and facilitates further reduction process. The metal carrier can guarantee good electrical conductivity, meanwhile the oxide cluster especially those reductive metal oxides can provide an electron rich environment, which can promote the adsorption and activation of reactant. However, it is also pointed out that the strong binding between O-containing species and Ti makes the OH* removal remain challenging [9]. Thus it is very important to design a novel catalyst for facile removal the OH*.

Based on the above analysis, the inverse CeO_x-based catalysts were constructed. For CeO_x/M (M = Cu, Ag, Au) catalyst, different amounts of electrons could be transferred from metal to oxide clusters, in the order of Cu > Ag > Au [6]. Herein, the $CeO_x/Ag(111)$ was employed, since it is relatively stable and its 4f states of Ce^{3+} has high activity [6]. Besides, detailed reaction mechanism of CO_2 electrochemical reduction to CO, HCOOH, CH_4 and CH_3OH has been systematically studied. The presence of Ce^{3+} generated by the SMSI effect between CeO_x and Ag reduces the free energy for the reduction of CO_2. Especially, it is beneficial to generate CH_3OH and CH_4 in thermodynamic. Different from other catalysts, the removal of OH is also facile, due to the weak interaction between H_2O and CeO_x cluster. Those results provide valuable reference to design more efficient catalysts for electrochemical reduction of CO_2.

2. Results and Discussion

2.1. Electronic Characteristics for the CeO_x/Ag(111) Catalyst

A Bader analysis of the charge was performed firstly for $CeO_x/Ag(111)$ catalyst, in order to reveal the electronic structure and interactions between ceria and Ag at the interface of this catalyst. As reported, the Bader charge of Ce in the particle is +2.00 e [5]. While the calculated Bader charge for Ce in the $CeO_2/Ag(111)$ are ~+2.1 e and ~+2.2 e, respectively (Table 1). Thus it can be inferred that the formal oxidation states of Ce atoms in the ceria cluster are +4 and +3, respectively [5]. Spin Density Difference (SDD) versus Z direction of the $CeO_x/Ag(111)$ catalyst is plotted in Fig. 1a, the isosurface of SDD is plotted in Figure 1b. From Figure 1a,b, obvious electron accumulation is founded on Ce atoms at the edge of a cluster. Therefore it can be concluded that the electrons are mainly located on the edge of the CeO_x cluster. In other words, single electrons are concentrated in certain areas of ceria cluster, the computational results show that only parts of Ce atoms which located on the edges of ceria cluster have been reduced (Figure 1b). All those Ce atoms can be considered as Ce^{3+}. In addition, the Electron Density Difference (EDD) versus Z direction of the $CeO_x/Ag(111)$ catalyst is plotted in Figure 2a, the isosurface of EDD is plotted in Figure 2b. From Figure 2, it was found that EDD indeed increased on CeO_x cluster and decreased on surface Ag atoms, which indicates that there is a charge transfer from the Ag slab to the ceria cluster. And the electrons are mainly coming from the surface Ag layer, which located under the CeO_x cluster, resulting in an oxidation of the Ag atoms and a reduction of the CeO_x cluster.

Table 1. Bader charge of the Ce and Ag atoms under the CeO_x cluster of CeO_x/Ag(111).

Bader Charge			
Ce	**Ag Atoms Under the CeO_x Cluster**		
2.18	0.07	−0.04	0.00
2.12	0.14	0.14	0.10
2.20	0.05	0.11	−0.02
2.11	0.08	0.10	−0.01
2.11	0.14	0.11	0.00
2.21	0.00	−0.01	−0.01
	0.00	0.14	0.01
	0.13	0.12	−0.01
	0.12	0.05	−0.03
	0.11	−0.02	−0.02
	0.10	0.11	
	0.11	0.16	

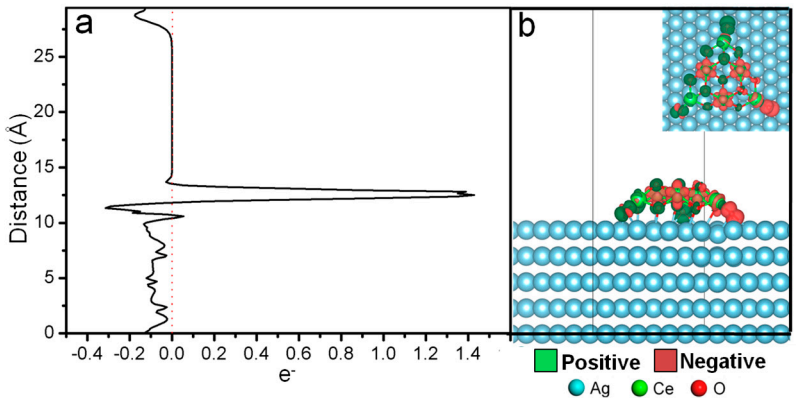

Figure 1. Spin density difference (SDD) of the CeO_x/Ag(111). (**a**) Spin Density Difference (SDD) versus Z direction of the CeO_x/Ag(111) catalyst, (**b**) Isosurfaces for single electron distribution.

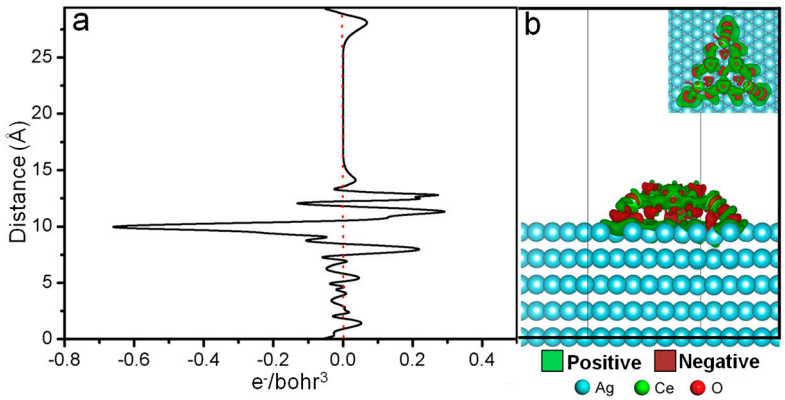

Figure 2. Electron density difference (EDD) of the CeO_x/Ag(111). (**a**) Electron density difference (EDD) versus Z direction of the CeO_x/Ag(111) catalyst, (**b**) Isosurfaces for EDD distribution.

2.2. CO_2 Adsorption and Activation

The adsorption and activation of CO_2 is considered as the first step for CO_2 reduction. In the initial CO_2 adsorption configurations, no matter where CO_2 was placed (on the interface of CeO_x/Ag(111), Ag and CeO_x, linear or bent structure). Only two stable structure of CO_2 adsorption (denoted as CO_2*, * = CeO_x/Ag(111)) were reached in the final (Figures 3 and 4c). CO_2 is linearly adsorbed on the edge (Ce^{3+}) or corner (Ce^{4+}) of the CeO_x cluster using its O atom. The adsorption energy of CO_2 for those two structures is 0.42 eV and 0.40 eV, respectively. The shortest distance between O atom of CO_2

and Ce atom of CeO_x cluster is 3.03 Å and 3.04 Å. Gradient isosurfaces of reduced density gradient (RDG) versus sign(λ_2)/ϱ (Figure 3a) [10] plot shows that there are Van Der Waals interactions between O-Ce and C-Ag for CO_2/*(Ce^{3+}) simultaneously. Whereas, in CO_2/*(Ce^{4+}), only O-Ce interaction has been found (Figure 3c). Spikes near zero in the corresponding scatter plot (Figure 3b,d) also reflect there exist weak interactions in CO_2/*(Ce^{3+}) than CO_2/*(Ce^{4+}). The synergism by Ag and CeO_x in CO_2/*(Ce^{3+}) configuration may be beneficial to the subsequent hydrogenating of CO_2. Therefore CO_2/*(Ce^{3+}) is chosen as the initial structure in this work.

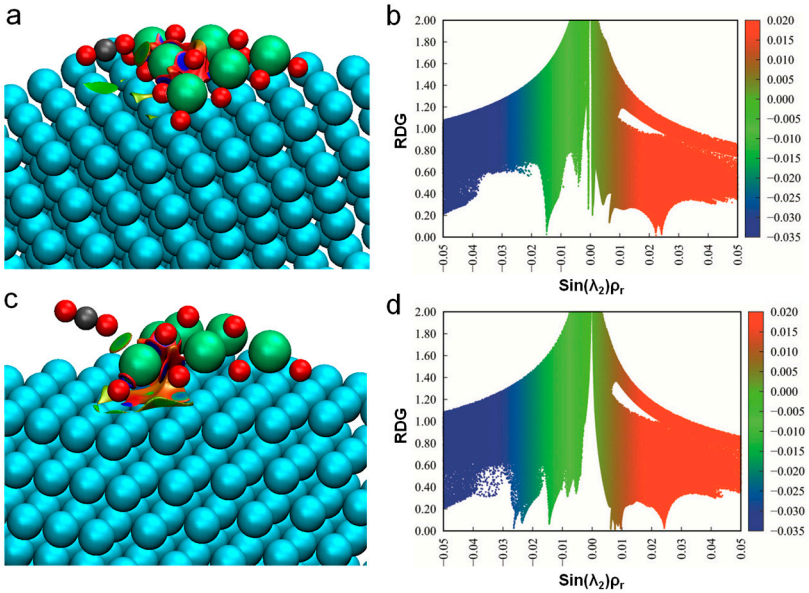

Figure 3. (**a**) Gradient isosurfaces for CO_2*(Ce^{3+}), (**b**) Scatter plot of RDG and sign(λ_2)/ϱ for CO_2*(Ce^{3+}), (**c**) Gradient isosurfaces for CO_2*(Ce^{4+}), (**d**) Scatter plot of RDG and sign(λ_2)/ϱ for CO_2*(Ce^{4+}). The surfaces are colored on a blue-green-red scale according to values of sign(λ_2)/ϱ, ranging from −0.05 to 0.05 au. Blue indicates strong attractive interactions, green indicates Van Der Waals interactions and red indicates strong nonbonded overlap.

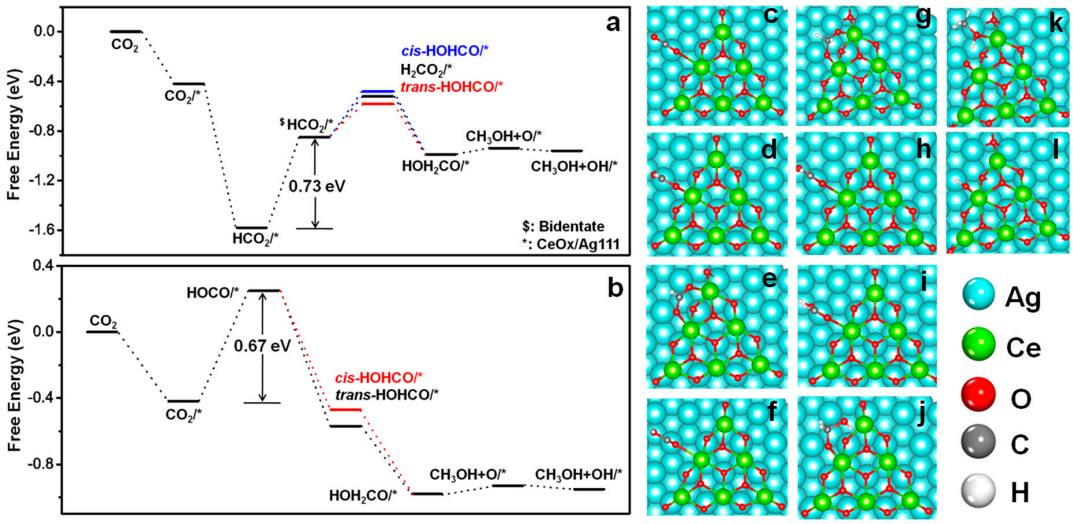

Figure 4. Free energy diagrams for the formation of formic acid and methanol. (**a**) HCO_2* path. (**b**) HOCO* path. (**c**–**l**) most stable structures for important stationary point involved in the formation of formic acid and methanol. (**c**) CO_2*, (**d**) HCO_2*, (**e**) HCO_2* (bidentate-coordination), (**f**) HOCO*, (**g**) H_2CO_2*, (**h**) trans-HOHCO, (**i**) *cis*-HOHCO, (**j**) HOH_2CO_2*, (**k**) (CH_3OH+O)*, (**l**) OH*. *: CeO_x/Ag(111) catalyst.

2.3. Formation of Formic Acid and Methanol

The CO_2 adsorption configuration shown in Figure 3a is set to be the starting point for further reduction. The first hydrogenation of CO_2* may occur at either the O or C atom, forming carboxyl (HOCO*) or formate (HCO_2*) species, respectively. Herein, the routes through both HOCO* and HCO_2* intermediates were investigated. The Gibbs free energy diagrams for all possible products involved in CO_2 reduction process on CeO_x/Ag(111) were also examined.

As mentioned above, hydrogenation of CO_2 could occur either on oxygen or carbon atom of CO_2. HOCO* or HCO_2* intermediates are eventually formed at the interface of CeO_x and Ag. The HCO_2* (Figure 4d) intermediate is formed with a free energy release of −1.14 eV (Figure 4a). While the HCO_2* intermediate can change to bidentate form using its O atoms with CeO_x cluster, which is endothermic with free energy barrier of 0.73 eV. When the hydrogenation of CO_2 occurs on the O atom (Figure 4b), forming HOCO* (Figure 4f) with a free energy barrier of 0.67 eV. This intermediate is bind to the catalyst using its C (C-Ag = 2.25 Å) and O (O-Ce = 2.56 Å) atom simultaneously. The Ag atom which bonds to C atom obviously migrates up from Ag surface. Obviously, the HCO_2* formation is thermodynamically preferable over HOCO*.

When HCO_2* or HOCO* intermediate is formed on the catalyst. Formic acid as an important product for CO_2 reduction can be generated firstly by hydrogenation of HCO_2* or HOCO* intermediate. For the hydrogenation of HOCO*, this is thermodynamically preferable. The formation of *cis*-HOHCO* and trans-HOHCO* (Figure 4h,i) is exothermic by 0.72 and 0.82 eV, respectively. For the hydrogenation of bidentate HCO_2*, subsequent reaction process can be achieved through two different ways. (a) The second hydrogen is bonded with carbon of HCO_2*, a H_2CO_2* intermediate is formed. The free energy change for this process is 0.42 eV endothermic. (b) The hydrogenation occurs on oxygen atom of HCO_2*, HOHCO* intermediate can be generated. There are also two possibilities here, (1) formation of *cis*-HOHCO* (0.47 eV, endothermic), (2) formation of trans-HOHCO* (0.37 eV, endothermic). The free energy change for the rate-limiting step of formic acid formation from HOCO* and HCO_2* intermediate are 0.67 and 0.73 eV, respectively. Obviously, HOCO* reaction path is slightly more facile for the formation of formic acid.

As shown in Figure 4, trans-HOHCO* can further hydrogenate by ($H^+ + e^-$) to generate HOH_2CO* intermediate. CH_3OH and O atom co-adsorbed on the catalyst can be generated through the further hydrogenation of HOH_2CO. Next, the formed CH_3OH can be desorbed from the surface of the catalyst, leaving only OH*. Thermodynamically, the formation of CH_3OH through HOH_2CO* is uphill in free energy by only 0.05 eV. In general, once HOHCO formed, it is very easy to convert into CH_3OH, although more hydrogenation steps are needed for this process.

2.4. Formation of Methane

With the aim of comparison, both HCO_2* and HOCH* reaction path have been plotted in Figure 5. When the hydrogenation of HOH_2CO* firstly occurs on the carbon atom, methoxy (CH_3O*) and hydroxyl (OH*) intermediates are formed and co-adsorbed on the catalyst. This process is endothermic with free energy change of 0.71 eV. Further hydrogenation for the formation of H_2O and CH_4 are all uphill with free energy barrier of 0.54 eV and 0.20 eV, respectively. Obviously, the total free energy change from CO_2* to CH_3OH and CH_4 are almost the same. Thus it is speculated that both CH_3OH and CH_4 are easy to form on the interface of this catalyst, as both of process are free energy downhill from the CO_2*. However, it is noteworthy that the formation of CH_4 needs more steps than that of CH_3OH. Thus, CH_3OH formation is probably facile than the formation of CH_4. The most endothermic steps for the formation of HOCO* or trans-HOHCO* are observed, which will be the potential-limiting steps for the formation of CH_3OH and CH_4 on the CeO_x/Ag(111) catalyst.

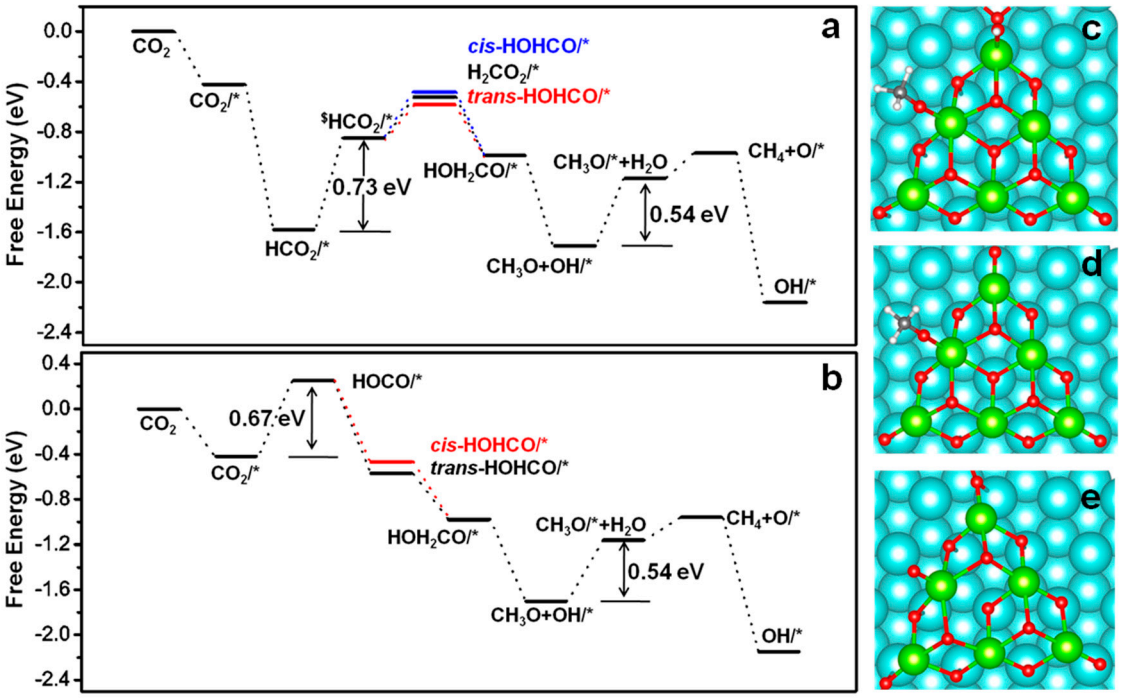

Figure 5. Free energy diagrams for the formation of methane. (**a**) HCO_2* path. (**b**) HOCO* path. (**c**–**e**) most stable structures for important stationary point involved in the formation of methane. (**c**) (CH_3O+OH)*, (**d**) CH_3*, (**e**) O*.

2.5. Formation of Carbon Monoxide

Although CO_2 only weakly binds to CeO_x/Ag(111), less energy is required for the formation of HOCO* from CO_2* than that on pure Ag [9], on which more than 1.2 eV is needed for the hydrogenating of CO_2 to form HOCO*. The formation of CO* (Figure 6b) from HOCO* is endothermic on CeO_x/Ag(111) with a free energy change of 0.69 eV. However, further hydrogenating of HOCO* is exothermic with a free energy change of −0.82 eV. Clearly, further hydrogenating of HOCO* to form HOHCO* is more facile on CeO_x/Ag(111) than the formation of CO (0.18 eV, CO*). Simultaneously, CO adsorption is quite stable on CeO_x/Ag(111). As CO desorption is endothermic with a free energy change of 0.83 eV. Consequently, CO* may be further reduced on CeO_x/Ag(111) to other products rather than desorbed from the catalyst. The reduction pathway and the free energy profile of the corresponding intermediates from CO* have been mapped out (Figure 6). As shown in Figure 6, apart from the formation of HCO* (0.25 eV), all other processes after HCO* formation are downhill in free energy.

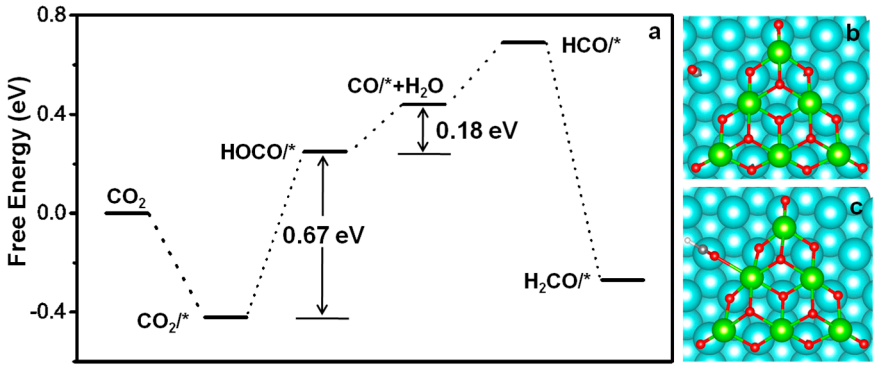

Figure 6. Free energy diagrams for the carbon monoxide. (**a**) reaction path for the formation of CO, (**b**) CO*, (**c**) HCO*.

As shown in Figure 6b, CO* is bonded to Ag only through C atom. Bond length of C-O and C-Ag are 1.15 and 2.15 Å, respectively. This indicates that CO is chemically adsorbed on the Ag surface and has been activated. With the formation of CHO*, O atom is weakly bonded to the Ce atom of the CeO_x cluster, distance of C-Ag and O-Ce are 2.20 and 2.60 Å. There is an obvious deformation of Ag surface. The Ag atom, which interacts with C atom, is moved upward from the Ag surface. Gradient isosurfaces of RDG and sign(λ_2)/ϱ [10] plot also shows clearly a strong attractive interaction between carbon and Ag (Figure S1). With further hydrogenating of CHO*, the formed CH_2O* bonds to CeO_x/Ag(111) only through O-Ce interaction (C-Ag 4.28 Å, O-Ce 2.71 Å). The C-Ag in CHO* is completely broken upon formation of CH_2O*. The same situation occurs in the formation of CH_3O*, in which methoxyl bonds to the CeO_x/Ag(111) only through O-Ce (C-Ag 6.14 Å, O-Ce 2.13 Å). The high oxygen affinity of CeO_x/Ag(111) keeps the O atom of CH_3O* bound to Ce strongly. And this, in turn, will cause the breaking of the C-O bond of CH_3O*. Eventually, CH_4 can be formed in the subsequent hydrogenation step.

2.6. Formation of Acetaldehyde

The formation of formaldehyde can be achieved through (a) hydrogenation of CO* and HCO*, which is mentioned above in 2.5, or (b) dehydrogenation of methoxy in the (CH_3O_OH)* intermediate. As plotted in Figure 7, Breaking C-O bond of HOH_2CO* intermediate can form CH_2O and OH co-adsorption intermediate (Figure 7c). With the formation H_2O, CH_2O* is ultimately formed. Free energy change for this process is 0.63 eV, which is slightly lower than the formation of HOCO*, thus the rate-limiting step for this reaction path is also the HOCO* generation. Besides, the dehydrogenation of CH_3O* intermediate can also lead to the formation of CH_2O* (0.88 eV). Obviously, this reaction path is relatively difficult to achieve. Compared with the formation of CH_3OH and CH_4, more energy is needed for the generation of CH_2O. Thus CH_2O formation is unfavorable on this catalyst.

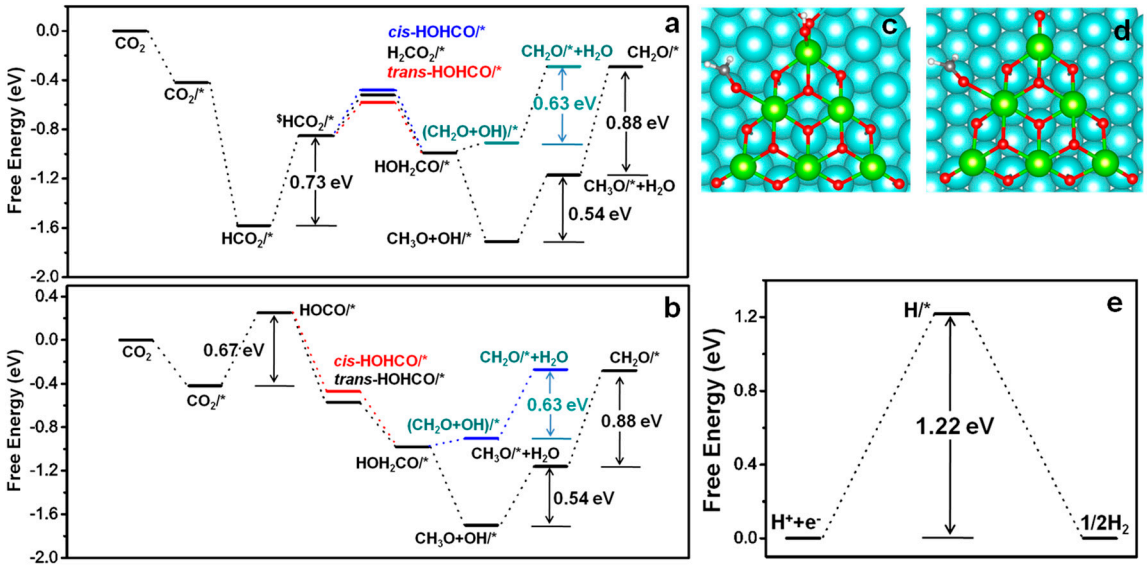

Figure 7. Free energy diagrams for the formation of acetaldehyde. (**a**) HCO_2* path. (**b**) HOCO* path. (**c**) (CH_2O+OH)*, (**d**) CH_2O*, (**e**) Hydrogen Evolution Reaction (HER) on CeO_x/Ag(111) catalyst.

To sustain the catalytic cycle, no matter in what kind of reaction path, the O* species has to be cleared through consecutive hydrogenating to OH* and further to H_2O. The hydrogenating of OH* to H_2O is endothermic, with a free energy barrier of 0.70 eV, which indicate that OH is the most stable intermediate species at U = 0 V. This makes OH removal become the free energy limiting step. However, the free energy change is still lower than the desorption energy (1 eV) needed on TiO_2/Ag

system [9] or pure metals (such as Pt (0.75 eV)) [11]. The free energy change needed for the formation and removal of H_2O is only slightly higher than the energy required for the generation of HOCO* intermediate (0.67 eV) on CeO_x/Ag(111) catalyst. The weak interaction between H_2O and CeO_x cluster is beneficial for the formation of H_2O (the distance of O-Ce has enlarged from 2.15 Å to 2.72 Å, for OH* and H_2O* intermediate), which makes the regeneration of the catalyst become easier, resulting in a great recyclability.

Finally, the hydrogen evolution reaction (HER), which is the main competitive reaction of CO_2RR, has been calculated. The computational result shows that the free energy change for the formation of H_2 is 1.22 eV, which is far higher than the rate-limiting step of CO_2RR on CeO_x/Ag(111) (Figure 7e). Based on all those advantages mentioned above, it is reasonable to believe that the CeO_x/Ag(111)is a potential excellent catalyst for CO_2 electroreduction.

The above analysis shows that CH_3OH and CH_4 are the main products on the surface of CeO_x/Ag(111) catalyst. In order to change into exothermic and spontaneous process for all the reaction steps, the free energy diagram with an external potential of −0.67 V (RHE) was depicted and shown in Figure 8. The potential is selected based on the potential-limiting step, that is the formation of HOCO*. Under this applied potential (U = −0.67 V vs RHE), the free energy change of all steps involving the proton-electron pairs will be corrected according to Equation (2). Under this potential, all steps following HOCO* formation become downhill on the free energy diagram.

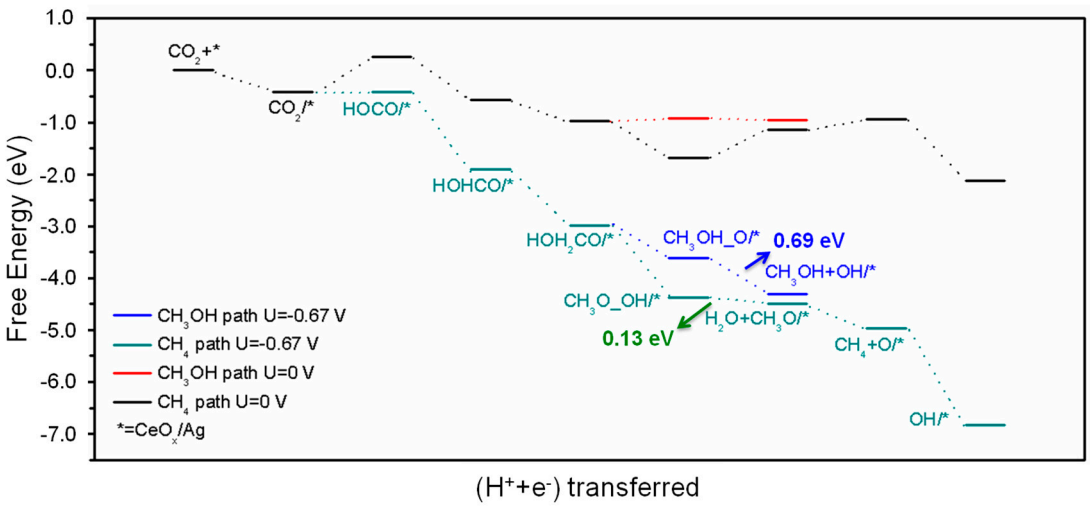

Figure 8. Free energy diagram for CO_2 reduction on CeO_x/Ag(111) along HOCO* pathway at −0.67 V (RHE).

When hydrogenation of CO_2 occurs on the oxygen atom, HOCO* is the key intermediate and plays a central role in the entire mechanism. Further hydrogenating HOCO* leads to the formation of HOHCO* (trans-formic acid) intermediate. When hydrogenation of CO_2 occurs on the carbon atom, trans-HOHCO becomes the critical intermediate. A HOH_2CO* intermediate can be formed through the hydrogenation of trans-HOHCO. Breaking different C-O bond of HOH_2CO* will lead to the formation of CH_3OH, CH_2O or an adsorbed methoxy (CH_3O*) species on the Ce site and an OH*. Subsequently, CH_3O* can be hydrogenated to produce CH_4 or CH_2O. And the catalyst will recover its original state with the desorption of H_2O by the hydrogenation of OH*. Based on the free energy profile for the HOCO* path shown in Figure 8, CH_3OH desorption from the catalyst release more energy (−0.69 eV) than the formation of CH_3O* (−0.13 eV), whereas, the CH_3O* intermediate is more stable (0.19 eV lower) than CH_3OH + OH*. This result indicates that CH_3OH formation is less favorite than CH_4 thermodynamically. However, CH_3OH formation requires fewer proton reduction and hydrogenation steps, therefore, both CH_3OH and CH_4 are likely to be generated.

3. Computational Details

Spin-polarized calculations are conducted with the Quickstep [12] module of the CP2K program package [12,13], which based on the Gaussian and plane waves formalism [14]. The exchange-correlation energy was described by the generalized-gradient approximation (GGA) with spin-polarized revised PBE functional (revPBE). In order to investigate the influence of dispersion, the structures and energies for all the stationary points included in our work are evaluated at the DFT-D3 level with the approximation suggested by Grimme [15] added to the revPBE calculated energy. Fronzi et. al have carried out studies on water adsorption on the stoichiometric and reduced CeO_2(111) surface [16]. They have pointed out that the DFT+U method has some inherent defects, such as no unique way to decide on what value to use for U; weather DFT+U method indeed provides a systematic improvement of the energetics of a system compared to plain DFT and so forth. Moreover, theoretical studies for the CO oxidation on $Au_xCe_{1-x}O_2$ catalyst also pointed out there is no hard evidence that GGA gives unusually large errors when used to calculate the energy differences [17]. In short, it is impossible to find a universal method which gives a satisfactory description of both the electronic structure and the energetics. Because this article focuses on the energy changes of the CO_2RR reaction process, Therefore DFT+U method is not considered in this paper. The wavefunctions were expanded in an optimized double-ζ Gaussian basis sets [16,18] with a cutoff energy of 500 Rydberg [14]. Core electrons have been modelled by scalar relativistic norm-conserving pseudo potentials [19] with 12, 6, 1, 4 and 11 valence electrons for Ce, O, H, C and Ag, respectively. Brillouin zone integration is performed with a reciprocal space mesh consisting of only the gamma point. Thermochemistry calculation is implemented by TAMkin [20], a post-processing toolkit for normal mode analysis. All other electronic property analyses deal with Multiwfn software, a program for realizing electronic wavefunction analysis [21].

The following equation was used to calculate the adsorption energy of an adsorbate

$$\Delta E_{ads} = E_{(adsorbate/(CeOx/Ag(111))} - E_{(adsorbate)} - E_{(CeOx/Ag(111))} \quad (1)$$

where $E_{(adsorbate/(CeOx/Ag(111))}$ is the total energy of an adsorbate bound to CeO_x/Ag(111), $E_{(adsorbate)}$ is the total energy of the isolated adsorbate and $E_{(CeOx/Ag(111))}$ is the total energy of bare CeO_x/Ag(111). A negative value of ΔE_{ads} corresponds to an exothermic adsorption process.

Spin Density Difference (SDD) and Electron Density Difference (EDD) for CeO_x/Ag(111) is computed by the following equation

$$SDD(EDD) = SD(ED)_{(CeOx/Ag(111))} - SD(ED)_{(CeOx)} - SD(ED)_{(Ag(111))}$$

where $SD(ED)_{(CeOx/Ag(111))}$ is the Spin Density (Electron Density) of the catalyst, $SD(ED)_{(CeOx)}$ and $SD(ED)_{(Ag(111))}$ are Spin Density (Electron Density) of CeO_x and Ag(111) respectively, the cartesian coordinates used for the computation of CeO_x and Ag(111) are consistent with that in the CeO_x/Ag(111).

The Gibbs free energy diagrams for CO_2 reduction along different pathways were calculated with reference to the computational hydrogen electrode (CHE) proposed by Nørskov et al. [22]. The free energy of each species is obtained using TAMKin (Table S1) [20]. The free energy change of each elementary step at external potential U will be shifted by eU as

$$\Delta G(U) = \Delta G(U = 0) + eU \quad (2)$$

where e is the electronic charge. According to Nørskov et al., the thermodynamic activation barrier equals the largest of the free energy differences [22].

A Ce_6O_{13} cluster, which is the most stable structure found by other theoretical work [6], is selected and supported on an Ag(111) metal surface described by means of 7 × 7, five atomic layers thick of Ag slab (245 Ag atoms) and a vacuum region of 20 Å between repeated slabs. In our calculations,

the atoms in the bottom two layers were fixed at their bulk position and those in the top four layers together with the supported CeO_x cluster and the adsorbates were allowed to relax.

4. Conclusions

The CeO_x/Ag(111) as a model of the metal supported metal oxide catalyst is constructed for electroreduction of CO_2. It is found that the transfer of electrons from top layer Ag atoms to CeO_x cluster leads to the reduction of Ce^{4+} to Ce^{3+} at the interface. Those interfacial Ce active sites could promote the adsorption and further reduction of CO_2. The dominating pathway on the CeO_x/Ag(111) catalyst to produce CH_3OH and CH_4 is via the HOH_2CO* intermediate, a key intermediate along both HOCO* or HCO_2* pathway. Once the HOH_2CO* is generated, the formation and desorption of CH_3OH and CH_4 is nearly thermal-neutrality. Nevertheless, the formation of acetaldehyde and CO is unfavorable. It is worth noting that the moderate binding of O-containing species makes OH* removal facile, resulting in a great recyclability of catalyst. The main competitive reaction (HER) has also been tested. Higher energy is needed for the formation of H_2 than that for the rate-limiting step of CO_2RR. Those results provide valuable reference to design more efficient catalysts for electrochemical reduction of CO_2.

Supplementary Materials: The following are available online at http://www.mdpi.com/2073-4344/9/1/22/s1. Figure S1: Gradient isosurfaces for CHO/*. The surfaces are colored on a blue-green-red scale according to values of sign(λ_2)/ϱ, ranging from −0.05 to 0.05 au. Blue indicates strong attractive interactions, green indicates Van Der Waals interactions and red indicates strong nonbonded overlap. Table S1: Free energy (kJ/mol) for all intermediates at different temperature (K). Cartesian coordinate for all stationary points involved in this work.

Author Contributions: Y.S. completed the main work of this manuscript. Z.X. wrote the manuscript.

Funding: This research was funded by the National Natural Science Foundation of China (21503028, 21506148).

Conflicts of Interest: The authors declare no conflict of interest. The founding sponsors had no role in the design of the study; in the collection, analyses, or interpretation of data; in the writing of the manuscript and in the decision to publish the results.

References

1. Tauster, S.J.; Fung, S.C.; Garten, R.L. Strong metal-support interactions. Group 8 noble metals supported on titanium dioxide. *J. Am. Chem. Soc.* **1978**, *100*, 170–175. [CrossRef]
2. Gonzalez-DelaCruz, V.M.; Holgado, J.P.; Pereñíguez, R.; Caballero, A. Morphology changes induced by strong metal-support interaction on a Ni-ceria catalytic system. *J. Catal.* **2008**, *257*, 307–314. [CrossRef]
3. Qin, Z.H.; Lewandowski, M.; Sun, Y.N.; Shaikhutdinov, S.; Freund, H.J. Encapsulation of Pt Nanoparticles as a Result of Strong Metal−Support Interaction with Fe_3O_4 (111). *J. Phys. Chem. C* **2008**, *112*, 10209–10213. [CrossRef]
4. Senanayake, S.D.; Ramírez, P.J.; Waluyo, I.; Kundu, S.; Mudiyanselage, K.; Liu, Z.; Liu, Z.; Axnanda, S.; Stacchiola, D.J.; Evans, J. Hydrogenation of CO_2 to Methanol on CeO_x/Cu(111) and ZnO/Cu(111) Catalysts: Role of the Metal–Oxide Interface and Importance of Ce^{3+} Sites. *J. Phys. Chem. C* **2016**, *120*, 1778–1784. [CrossRef]
5. Yang, F.; Graciani, J.; Evans, J.; Liu, P.; Hrbek, J.; Sanz, J.F.; Rodriguez, J.A. CO oxidation on inverse CeO_x/Cu(111) catalysts: High catalytic activity and ceria-promoted dissociation of O_2. *J. Am. Chem. Soc.* **2011**, *133*, 3444–3451. [CrossRef] [PubMed]
6. Graciani, J.; Vidal, A.B.; Rodriguez, J.A.; Sanz, J.F. Unraveling the Nature of the Oxide–Metal Interaction in Ceria-Based Noble Metal Inverse Catalysts. *J. Phys. Chem. C* **2014**, *118*, 26931–26938. [CrossRef]
7. Rodriguez, J.A.; Graciani, J.; Evans, J.; Park, J.B.; Yang, F.; Stacchiola, D.; Senanayake, S.D.; Ma, S.; Pérez, M.; Liu, P.; et al. Water-Gas Shift Reaction on a Highly Active Inverse CeO_x/Cu(111) Catalyst: Unique Role of Ceria Nanoparticles. *Angew. Chem. Int. Edit.* **2009**, *48*, 8047–8050. [CrossRef]
8. Graciani, J.; Mudiyanselage, K.; Xu, F.; Baber, A.E.; Evans, J.; Senanayake, S.D.; Stacchiola, D.J.; Liu, P.; Hrbek, J.; Sanz, J.F.; et al. Highly active copper-ceria and copper-ceria-titania catalysts for methanol synthesis from CO_2. *Science* **2014**, *345*, 546–550. [CrossRef]

9. Zhai, L.; Cui, C.; Zhao, Y.; Zhu, X.; Han, J.; Wang, H.; Ge, Q. Titania-Modified Ag Electrocatalyst for Selective CO_2 Reduction to CH_3OH and CH_4 from DFT Study. *J. Phys. Chem. C* **2017**, *121*, 16275–16282. [CrossRef]
10. Johnson, E.R.; Keinan, S.; Mori-Sánchez, P.; Contreras-García, J.; Cohen, A.J.; Yang, W. Revealing noncovalent interactions. *J. Am. Chem. Soc.* **2010**, *132*, 6498–6506. [CrossRef]
11. Keith, J.A.; Jacob, T. Theoretical Studies of Potential-Dependent and Competing Mechanisms of the Electrocatalytic Oxygen Reduction Reaction on Pt(111). *Angew. Chem. Int. Edit.* **2010**, *49*, 9521–9525. [CrossRef]
12. Vandevondele, J.; Krack, M.; Mohamed, F.; Parrinello, M.; Chassaing, T.; Hutter, J. Quickstep: Fast and accurate density functional calculations using a mixed Gaussian and plane waves approach. *Comput. Phys. Commun.* **2005**, *167*, 103–128. [CrossRef]
13. CP2K Version 4.1. CP2K Is Freely. Available online: www.cp2k.org (accessed on 15 October 2015).
14. Geraldlippert, B.; Huttermicheleparrinello, J. A hybrid Gaussian and plane wave density functional scheme. *Mol. Phys.* **1997**, *92*, 477–488. [CrossRef]
15. Grimme, S.; Antony, J.; Ehrlich, S.; Krieg, H. A consistent and accurate ab initio parametrization of density functional dispersion correction (DFT-D) for the 94 elements H-Pu. *J. Chem. Phys.* **2010**, *132*, 154104–154119. [CrossRef] [PubMed]
16. Fronzi, M.; Piccinin, S.; Delley, B.; Traversa, E.; Stampfl, C. Water adsorption on the stoichiometric and reduced CeO_2(111) surface: A first-principles investigation. *Phys. Chem. Chem. Phys.* **2009**, *11*, 9188–9199. [CrossRef] [PubMed]
17. Shapovalov, V.; Metiu, H. Catalysis by doped oxides: CO oxidation by $Au_xCe_{1-x}O_2$. *J. Catal.* **2007**, *245*, 205–214. [CrossRef]
18. Wang, Y.G.; Mei, D.; Li, J.; Rousseau, R. DFT+U Study on the Localized Electronic States and Their Potential Role during H_2O Dissociation and CO Oxidation Processes on CeO_2(111) Surface. *J. Phys. Chem. C* **2015**, *117*, 23082–23089. [CrossRef]
19. Goedecker, S.; Teter, M.; Hutter, J. Separable dual-space Gaussian pseudopotentials. *Phys. Rev. B* **1995**, *54*, 1703–1710. [CrossRef]
20. Ghysels, A.; Verstraelen, T.; Hemelsoet, K.; Waroquier, M.; Van, S.V. TAMkin: A versatile package for vibrational analysis and chemical kinetics. *J. Chem. Inf. Model.* **2010**, *50*, 1736–1750. [CrossRef]
21. Lu, T.; Chen, F. Multiwfn: A multifunctional wavefunction analyzer. *J. Comput. Chem.* **2012**, *33*, 580–592. [CrossRef]
22. Nørskov, J.K.; Rossmeisl, J.; Logadottir, A.; Lindqvist, L.; Kitchin, J.R.; Bligaard, T.; Jónsson, H. Origin of the Overpotential for Oxygen Reduction at a Fuel-Cell Cathode. *J. Phys. Chem. B* **2004**, *108*, 17886–17892. [CrossRef]